Boron-doped Graphene Synthesis by Pulsed Laser Co-Deposition of Carbon and Boron

Y. Bleu, F. Bourquard, V. Barnier, Y. Lefkir, A.-S. Loir, F. Garrelie, C. Donnet, Stéphanie Reynaud

Boron-doped Graphene Synthesis by Pulsed Laser Co-Deposition of Carbon and Boron

Y. Bleu[1], F. Bourquard[1], V. Barnier[2], Y. Lefkir[1], S. Reynaud[1], A.-S. Loir[1], F. Garrelie[1], C. Donnet[1(*)]

(1) Univ. Lyon, Laboratoire Hubert Curien UMR 5516 CNRS, Université Jean Monnet, F-42000 Saint-Étienne, France

(2) Université de Lyon, Mines Saint-Etienne, CNRS, Laboratoire Georges Friedel UMR 5307 CNRS, F-42023 Saint-Etienne, France

(*) Corresponding author: Christophe.Donnet@univ-st-etienne.fr

Abstract

Incorporating dopants, such as boron, in graphene, is crucial for many applications in electrochemistry, sensors, photovoltaics, and catalysis. Many routes have been investigated for the preparation of B-doped graphene (BG) films, including chemical processes. A different way to obtain boron-doped layers to better control the concentration of boron in the doped graphene film, is pulsed laser co-ablation of C and B solid sources followed by rapid thermal heating of the B-doped carbon film deposited on a metal catalyst. Amorphous a-C:B films, containing 2%at. boron, are synthetized by pulse laser deposition onto a nickel film catalyst. Rapid thermal annealing at 1100°C leads to the formation of boron-doped graphene films, characterized by Raman, XPS, FEG-SEM, HRTEM and AFM. The results confirm the production of 1-4 layer boron doped graphene films, with a similar 2 at.% boron concentration to that of the a-C:B used as the graphene solid precursor. Boron doping does not modify the nano-architecture of graphene, but increases the concentration of defects in the films. Our results pave a new way for boron doped graphene synthesis using laser processing in a controlled and reproducible way, in particular to achieve designed electrical and chemical properties in various electronic and electrochemical applications.

1. Introduction

Recent studies focus on doping graphene nanosheets with various heteroatoms, in particular, to modulate the band gap and tune the electronic, physical-chemical, optical and structural properties of graphene, as reviewed, for example, by Wang et al. for boron, nitrogen, phosphorus, group VIa (O, S) and group VIIa (F, Cl, Br, I) doping elements**[1]**. More recently, Agnoli et al.**[2]** published an almost complete review on boron-doped graphene (BG) films, highlighting both theoretical and experimental studies on structure and properties, as well as synthesis routes and emerging applications in several fields including electrochemistry, sensors, photovoltaics, catalysis, and biology. Boron is an interesting doping element to extend most graphene film properties and is certainly less investigated than nitrogen, indeed, as shown by DFT calculations, boron can displace carbon atoms from the lattice more efficiently**[3]**. Incorporating boron in the carbon hexagonal lattice of graphene increases the concentration of holes, and, compared to C, the electron-deficient nature of B has a p-doping effect, with a downshift of the Fermi level (decrease of 0.65 eV with 2 at.% of boron) towards the Dirac point**[4]**. Boron atoms form sp^2 hybridization in the carbon lattice, thus retaining the planar structure of graphene, and in-plane BC_3 substitutional doping appears to be the most stable configuration. Since B-C bonds are slightly longer than C-C bonds in graphene, lower strain energy is induced by substitutional boron doping, and the substitution is thus easier to compare with in-plane nitrogen doping. Due to the strong B-C bond energy, the mechanical properties of graphene are preserved but the thermal conductivity of boron-doped graphene (BG) is dramatically reduced compared to pristine graphene.

Many routes have been investigated for the preparation of boron-doped graphene (BG) films, including liquid state synthesis, solid phase synthesis, and chemical Vapor Deposition (CVD) synthesis. Liquid phase synthesis includes hydrothermal and solvothermal processes combining liquid precursors as carbon and boron sources**[5]** or combining solid carbon-based precursor (such as graphene oxide, GO) with liquid boron-based precursors**[6–8]**. Solid state synthesis includes arc discharge of graphene electrodes in the presence of diborane (probably the first synthesis or BG**[9]**, exfoliation of BG sheets synthetized by chemical reactions between graphene or graphene oxide with various boron precursors**[10–18]**, high temperature sublimation of a single crystal of highly boron-doped SiC**[19]** and thermal decomposition of B_4C**[20]**. CVD processes, have been widely and successfully used for high

quality graphene synthesis on large areas, and also with various boron sources, to produce BG films**[21–29]**. In most published works, the well-known mechanism of (doped-) graphene synthesis is based on carbon dissolution in the Ni catalyst at high temperature, followed by precipitation of graphene layers upon cooling. Whatever the process, boron contents (when quantified) generally range between 1% and 6 at.% in most BG films. In the case of CVD processes, the major challenges are (i) the formation of metal boride compounds on the catalytic substrate**[22,25]**, and (ii) the need for rather high B/C ratios in the stream precursor (compared to the B/C ratio in the resulting BG film) to overcome the hindered kinetics of boron incorporation in graphene lattice**[3,22]**. Indeed, Cattelan et al.**[22]** noted that all attempts to deposit BG layers in one step have been unsuccessful, to the formation of very reactive boron species on the metal catalyst. To the best of our knowledge, only one paper**[30]**, published in 2018, reports BG film synthesis from both carbon and boron solid sources, by molecular beam epitaxy on alumina substrates. Boron concentrations ranging from 7.6 to 10 at. % (depending on the process parameters) were achieved, and a significant effect of boron incorporation on the charge carrier concentration and on mobility was observed.

The present proof is probably the first attempt to use carbon and boron solid precursors ablated by pulsed laser in a controlled way, to address the composition and nanostructure of BG films. The process is based on pulsed laser (co-)deposition (PLD) of carbon and boron, which has already been investigated to obtain pure graphene films (see our recent review**[31]**, and nitrogen-doped graphene films (NG)**[32,33]**. We have already demonstrated the ability of PLD to obtain boron-doped diamond-like carbon films (a-C:B)**[34]**, providing the foundation to extend the process for BG film synthesis developed in the present work. Contrary to what is usually observed with CVD synthesis, by PLD, we observed a similar boron content in the boron-doped carbon precursor and in the final boron-doped graphene, which is a real advantage for doped graphene synthesis in terms of process reliability. The present contribution investigates for the first time the ability of PLD to produce BG films and to correlate the synthesis process with the nanoarchitecture and composition of the BG films.

2. Experimental

The synthesis process of pulsed laser co-deposition is depicted in **Figure 1**. SiO_2 substrates were ultrasonically cleaned (in acetone then in ethanol and deionized water baths). Then, a

60 nm thick nickel (Ni) film was deposited by thermal evaporation on the top of the SiO_2 substrate in a vacuum chamber pumped at a base pressure of 10^{-4} Pa. High purity (99.99%) Ni was melted thermally in a tungsten nacelle and evaporated towards the substrate (**Figure 1a**). The deposition rate was set at 1.5 nm/minute to minimize residual stress in the growing film, thereby limiting film delamination. Subsequently, the Ni(60 nm)/SiO_2 substrate was introduced in a vacuum PLD chamber pumped at a base pressure of 10^{-4} Pa and mounted on a sample holder placed at a distance of 40 mm from the target holders (**Figure 1b**). Ablation was operated at room temperature by an excimer laser KrF with 248 nm wavelength, a pulse duration of 20 ns, a repetition rate of 10 Hz an energy per pulse of 120 mJ. The energy density (fluence) of the laser beam was kept constant at 2.7 J/cm^2. In such conditions, the ablation rates of the carbon (99.997%) and boron (99%) were 5.0 nm.mn^{-1} and 0.4 nm.mn^{-1}, respectively. A sequence of co-ablation was defined to deposit 0.3 nm of a diluted mixture of boron and carbon atoms, repeated 33 times in order to reach an a-C: B film thickness of about 10 nm, aiming for a boron concentration of 2% atomic. Systematically, the last ablated species was carbon. A pure a-C film of similar thickness was also deposited on Ni(60 nm) /SiO_2 for the purpose of comparison. The last step consisted in heating the a-C:B/Ni/SiO_2 film to 1100 °C for 2 minutes at a vacuum pressure of 10^3 Pa in a rapid thermal annealing (RTA) oven with a heating ramp rate of 15 °C/s and a cooling rate of about 1°C/s (**Figure 1c**). The RTA oven had a small heat capacity thereby allowing rapid cooling. A pyrometer (calibrated by a thermocouple in contact with the substrate) measured the heating temperature on the backside of the sample holder.

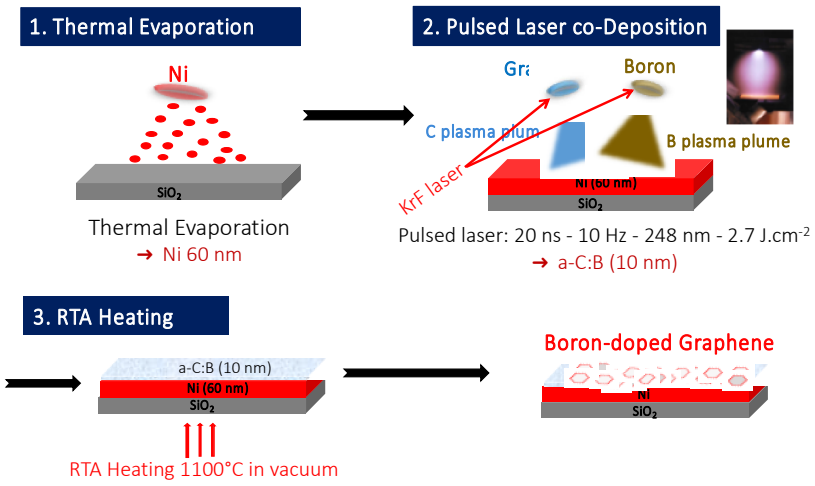

Figure 1: Synthesis route of boron-doped graphene films obtained by combining pulsed laser co-deposition (PLD) of carbon and boron, with rapid thermal annealing (RTA).

Raman spectroscopy was performed using an Aramis Jobin Yvon spectrometer at 442 nm (2.81 eV), with a spectral resolution of 2 cm^{-1} and a lateral resolution of ~1 µm. The laser beam was focused on the sample with a x100 objective and the laser power was kept below 3 mW to avoid damaging the surface of the film. The diameter of the laser beam was estimated to be near 1 micrometer, near the diffraction limit at this wavelength. Raman components were associated with a Lorentzian fit, safe for the asymmetric G peak, which was fitted using a Breit-Wigner-Fano function. A custom fitting function was computed for all recorded spectra, and a simple linear function was added to eliminate the background. This enabled access to the exact values of the various peak positions, widths, and maximum peak height intensities. Raman maps were built from the acquisition of each 1 micrometer spectrum, over probed surfaces measuring 10 × 10 square micrometers. Scanning electron microscopy (SEM) images were recorded using a FEI Novanano SEM 200 operated at 15kV. X-ray photoelectron spectroscopy (XPS) was performed with a Thermo VG Theta probe spectrometer (Thermo Fisher Scientific) equipped with a focused monochromatic AlKα source (hν = 1486.68 eV, 400 µm spot size). Photoelectrons were analyzed using a concentric hemispherical analyzer operating in a constant ΔE mode. For all the samples analyzed, narrow scans were recorded for C1s and B1s with a step size of 0.1 eV and pass energy of 50 eV. High Resolution Transmission Microscopy (HRTEM) was performed by using a JEOL NEO ARM microscope, equipped with a spherical aberration corrector, operating at an acceleration voltage of 60 kV and an emission current of 10 µA. Boron-doped graphene sheets were collected on a holey carbon copper grid which was maintained at liquid nitrogen temperature during analysis, to minimize damages induced by the electron beam. The spatial resolution is lower than 0.1 nm. Atomic Force microscopy (AFM) measurements were performed using AGILENT 5500 microscope operating in tapping mode in the ambient environment at room temperature. All the images were obtained at 1 Hz, 512 x 512 pixels (image definition). The AFM image treatment and root mean square roughness (RMS) were determined with Gwyddion software.

3. Results and discussion

Figure 2a shows a typical chip of boron-doped graphene observed by HRTEM. Such typical chip contains several superimposed sheets of graphene, as seen by areas with different contrasts. Indeed, graphene may contain residual stress leading to twisting and winding of the sheets after extraction from the SiO_2 substrate to the HRTEM copper grid. As a consequence,

it was extremely difficult to observe areas with only one sheet containing few layers of graphene. **Figure 2b** shows a high-resolution image of such an area, constituted of four superimposed boron-doped layers, with a typical distance of 0.3 nm between the carbon planes.

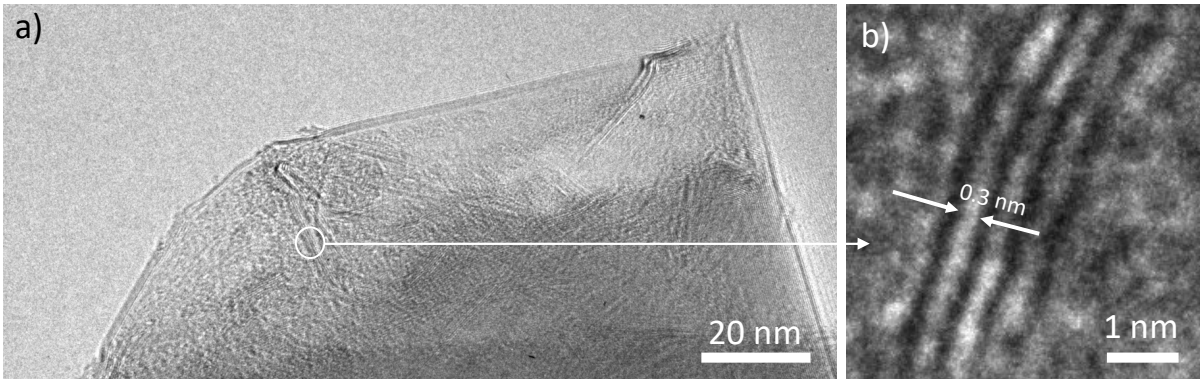

Figure 2: a) HRTEM investigation of a typical chip of boron-doped graphene; b) detail on a zone containing a few-layer graphene sheet.

Raman investigations of the graphene and boron-doped graphene (BG) revealed the usual G, D and 2D bands that are characteristic of few-layer graphene containing defects. Our interpretations of the Raman features are based on previously published data**[35–37]**. The G band (near 1580 cm^{-1}) is associated with covalent C-C bonding vibration in the graphitic matrix and is present in all carbon materials containing sp^2 bonding. The D band (near 1360 cm^{-1}) is associated with aromatic circle pulsation ("breathing mode") and only appears in the presence of defects and dislocations in the graphitic matrix. The 2D band (near 2730 cm^{-1}) is associated with a double resonance Raman scattering process between two aromatic rings, and its deconvolution enables estimation of the number of graphene layers, which is mainly within the 1-5 range. Moreover, the 2D/G intensity ratio is a good indicator of the graphene-like quality of a thin film. Additional D + D", D + D' and 2D' bands may be also observed. The D + D" and 2D' emerge, like the 2D peak, as a combination of two phonon modes individually associated with defects (D' and D") that allow aromatic ring breathing in carbon materials. The combination of those resonances may appear without defects as the two phonons can verify momentum conservation provided they have opposite wavevectors. In the case of the D + D' band, sometimes labelled D + G, the excitation mechanisms are not yet completely clear, but whether it is a combination of D and G phonons or D and D' does not alter the fact that either one or both phonons require a defect to arise. Thus, the D + D' band mostly appears in defective graphene-like material.

Figure 3 shows RAMAN mapping of the G and 2D positions, both related to undoped graphene and BG films. **Figure 4** shows RAMAN mapping of 2D/G ratio, D/G ratio and 2D full width at half maximum (FWHM) of both films. Such 10x10 μm^2 areas are typical of the whole graphene film surfaces. **Figure 5** shows two Raman spectra, extracted from the maps in **Figures 3-4**. They are linked with two distinct representative probed areas (1 µm diameter corresponding to the laser spot size), labelled spots "A" and "B" on the maps. The corresponding Raman characteristics of each spectrum are listed in **Table 1**. For the BG film, deconvolution of the 2D band related to both spots "A" and "B" are detailed in **Figure 6.** On these typical spectra extracted from the mappings, the 2D/G ratio is not significantly affected by the boron doping, as well as the G and D band shifts. This may be due to the rather low concentration of dopants. However, the D/G ratio is significantly increased by a factor 4 (spot A) and 5 (spot B), which is consistent with a strong reduction of the carbon cluster size and increase of defect density. We conclude that the effect of the incorporation of a rather small concentration of dopant mainly affects the defective nature of the graphene film, without modifying significantly the graphene layer architecture.

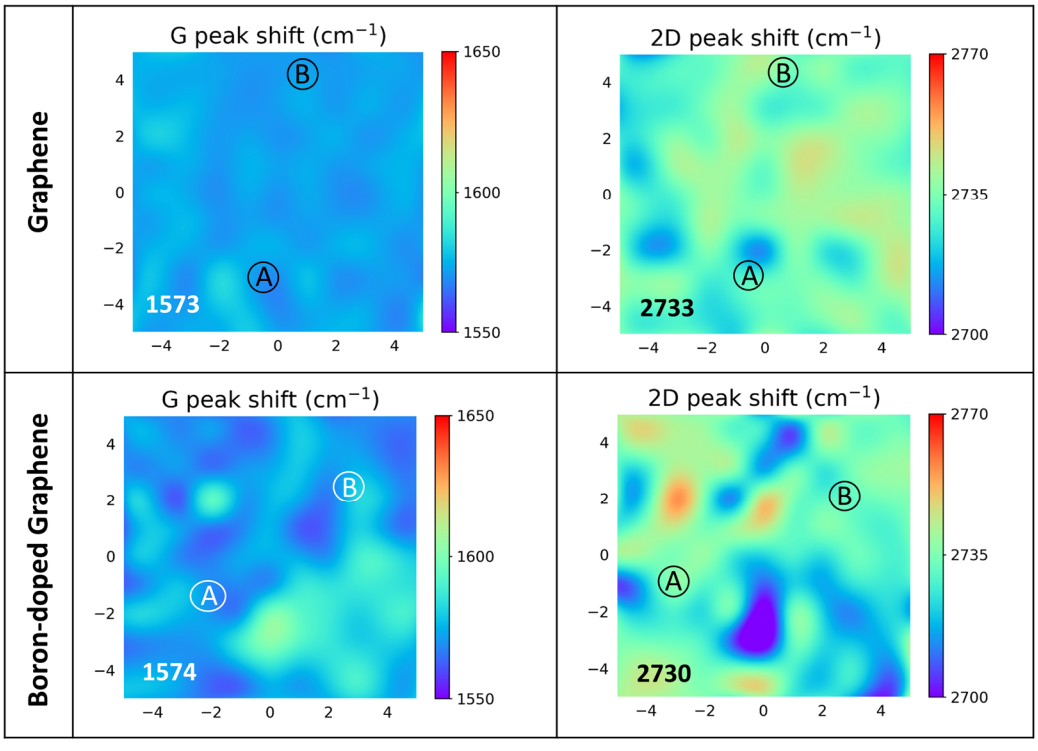

Figure 3: Raman mapping (10x10 μm^2) showing Raman G and 2D peak shifts of graphene and boron-doped graphene. "A" and "B" labels refer to areas whose RAMAN spectra are depicted in Fig.4.c. The average values of the G and 2D band positions related to the probed areas are indicated bottom left on each map. The low concentration of boron dopant does not affect the G and 2D band positions.

The average positions of both G and 2D bands, similar for the graphene and BG film, observed on areas A and B (Figure 5), are confirmed on the mapping (**Figure 3**) with a similar average band shift of 1573 and 1574 cm^{-1} for the D band, and 2733 and 2730 cm^{-1} for the G band, respectively. However, in some areas, such as spot "A" related to the BG film, a significant G band blue shift up to 12 cm^{-1} is observed compared to the average value of the mapping. Such a G band blueshift is frequently observed in BG films obtained using other synthesis methods**[21–23]** and is frequently associated with an increase in the D/G ratio consistent with a substantial decrease in cluster size. Incorporating boron in the graphene sheets leads to a moderate increase in the 2D/G ratio (from 0.63 to 0.78) together with a significant increase in the D/G ratio (from 0.15 to 0.41) as can be seen in **Figure 4**. These values are average values of the ratios calculated from the 100 Raman spectra accumulated to build each map. Note that some areas on the map of the BG film exhibit 2D/G ratios slightly higher than 1. The D/G ratio is an indication of disorder in carbonaceous structures and in the size of the graphene crystallite. From the Tuinstra-Kœnig relation**[38]**, one deduces average values of in-plane correlation lengths of 59 nm for the graphene film and 22 nm for the BG film. Thus, incorporating boron increases the disorder of the carbonaceous structure and reduces the size of the crystallite compared to undoped graphene. Lateral inhomogeneity of the G and 2D band positions, as well as of both 2D/G and D/G ratios, is more pronounced in the BG film than in the graphene film. The average full width at half maximum (FWHM) is similar for both films, 76-77 cm^{-1}, which mainly corresponds to tri-layer graphene, as typically observed with the 2D deconvolution of spot "B" related to BG (**Figure 6**) with 6 Lorentzian contributions (FWHM of about 30 cm^{-1} each). We also observed that the 2D bands related to tri-layer graphene (spot "B") are rather symmetric, which is consistent with ABA stacking in both the undoped and BG graphene films**[39]**. However, some probed areas are typical of bi-layer graphene, as is the case of the 2D deconvolution of spot "A" related to BG (**Figure 6**), with 4 Lorentzian contributions. These two-layer areas systematically exhibit a higher 2D/G ratio with a similar D/G ratio, meaning that the defect content is similar whatever the number of layers.

To evaluate the distribution of the layer number on the surface of the BG film more precisely, a statistical analysis was performed by combining the I_{2D}/I_G and FWHM(2D) values deduced from the 100 spectra recorded on the selected representative area. This analysis quantified the distribution of the I_{2D}/I_G and FWHM(2D) values between their minimum and maximum values. From data depicted on **Figure 7**:

- If one considers the statistical distribution of I_{2D}/I_G (**Figure 7a**), the I_{2D}/I_G ratios of 3% of the probed area were higher than 1.4, 74% were between 0.7 and 1.4, and 23% were higher than 0.6. Based on the literature, this is consistent with 74% of the probed area with 2-3 layers of BG.
- If one considers the statistical distribution of FWHM(2D) (**Figure 7b**), 9% of the probed area had FWHM(2D) values between 30 and 60 cm^{-1}, 61% between 70 and 80 cm^{-1}, and 30% higher than 90 cm^{-1}. Based on the literature, this is consistent with 69% of the probed area with 2-3 layers of BG.

Both statistical evaluations demonstrate that the BG film mainly comprises 2-3 layers of boron-doped graphene, as illustrated in **Figure 7c** showing the distribution of FWHM(2D) versus I_{2D}/I_G.

An important conclusion from these Raman characterizations is that the only real difference between the BG and graphene responses is the D band intensity. Looking only at the G and 2D features, it seems that boron doping (at the levels proposed here) affects neither the number of graphene layers nor the stacking of the layers. Only the number of defects in the graphene-like matrix increases. This is opposite of what we observed when we were synthesizing nitrogen doped graphene in a similar setup**[32,33]**. However, the comparison with those already published results remains difficult due to a significant difference of heating temperature used for synthesis of our N- and B-doped graphene. Nevertheless, for the boron doped graphene obtained in the present work, the significant increase of defect concentration, deduced from the increase of the D/G intensity ratio compared to the undoped film, may be interesting in applications many when tailoring the electrical and chemical properties of graphene, for electrochemical devices for example.

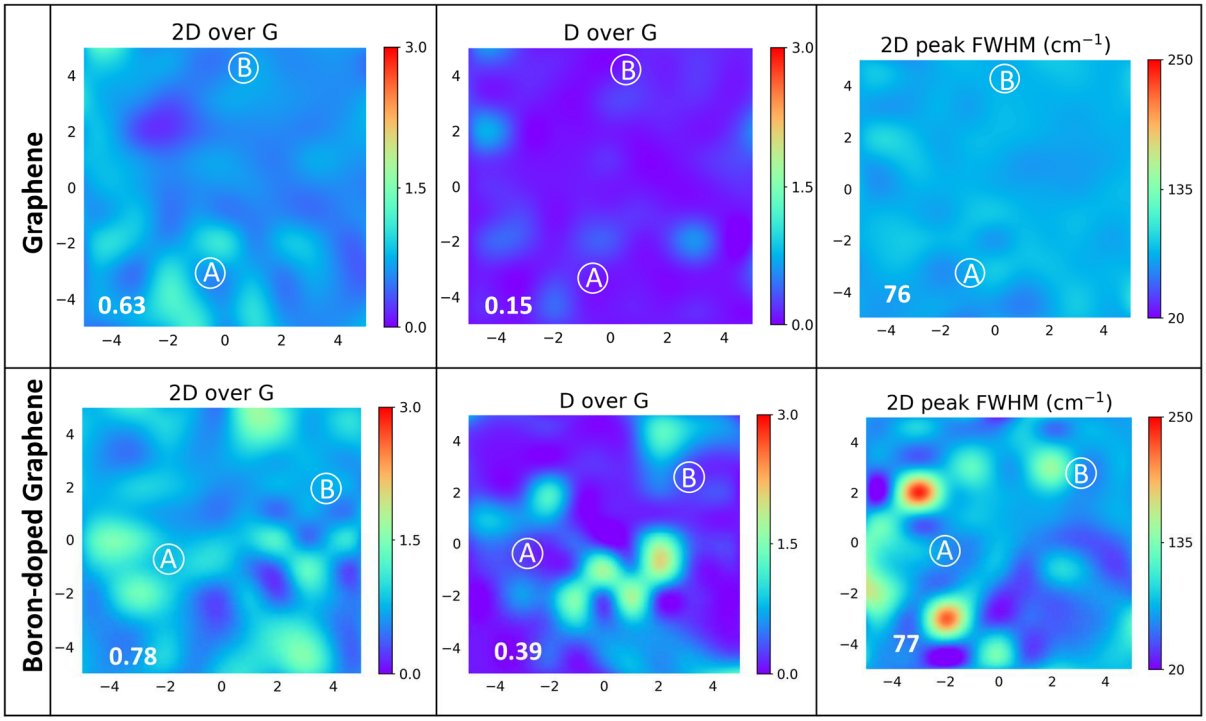

Figure 4: Raman mapping (10x10 µm^2) showing 2D/G and D/G intensity ratios, and 2D FWHM of graphene and boron-doped graphene. Labels “A” and “B” refer to areas whose RAMAN spectra are depicted in Fig.4. The average values 2D/G, D/G and 2D FWHM related to the probed areas are indicated bottom left on each map.

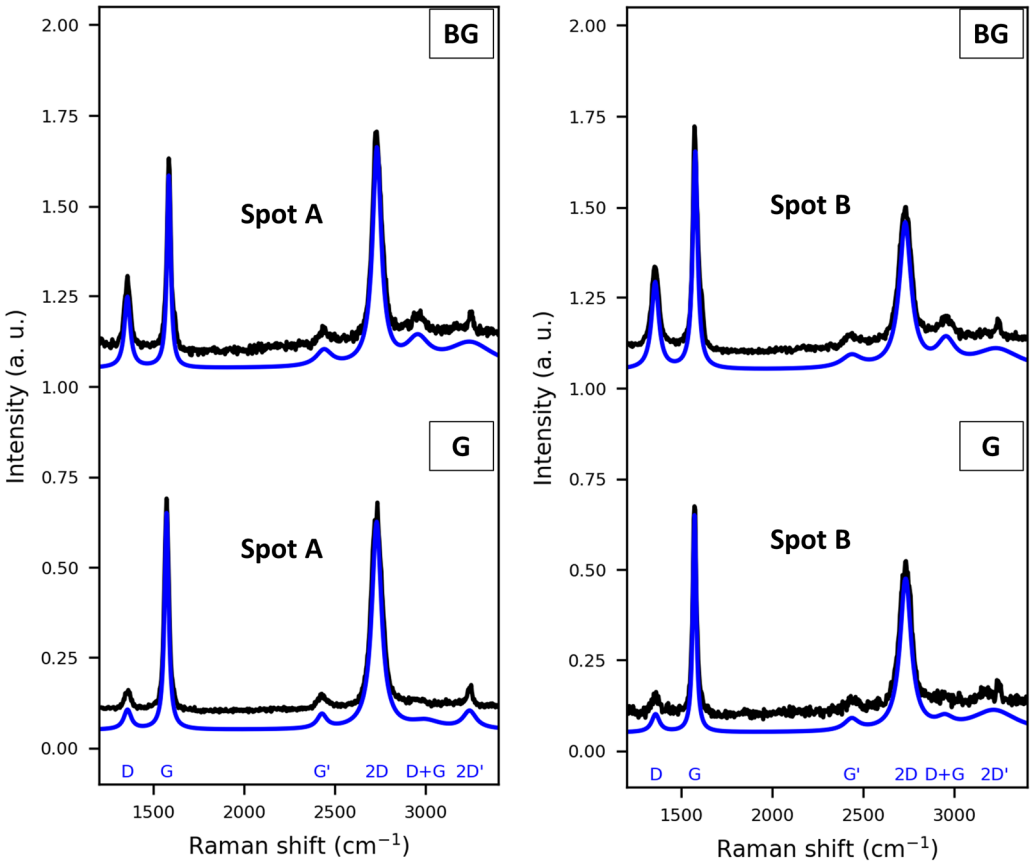

Figure 5: Raman spectra of graphene (G) and boron-doped graphene (BG), related to spot A and spot B shown in the Raman mappings in Figs.3 and 4. The black curves show the experimental spectra. The blue curves show the superimposed simulated spectra obtained with the procedure described in the experimental section.

	Graphene		Boron-doped Graphene	
	Spot A (~bilayer)	Spot B (~trilayer)	Spot A (~bilayer)	Spot B (~trilayer)
I(2D)/I(G)	0.96	0.69	1.12	0.66
I(D)/I(G)	0.09	0.08	0.37	0.40
La (nm)	102	115	25	23
2D position (cm^{-1})	2731	2733	2732	2730
2D FWHM (cm^{-1})	64	73	57	76
G position (cm^{-1})	1574	1574	1586	1577
D position (cm^{-1})	1358	1360	1357	1352

Table 1: Raman characteristics deduced from the two spectra depicted in Fig.5, and extracted from the mappings in Fig.3-4.

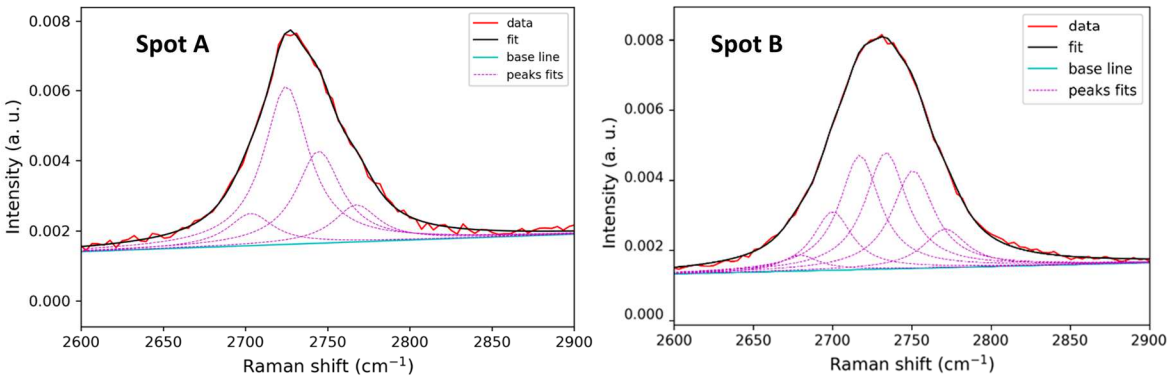

Figure 6: RAMAN 2D band of boron-doped graphene (BG) extracted from Raman spectra depicted in Fig.5, and related to spot A and spot B shown in Raman mappings in Figs.3 and 4. The 2D bands related to spot A and spot B are fitted with 4 and 6 elementary Lorentzian contributions (with a FWHM of about 30 cm^{-1}), consistent with a bilayer and trilayer graphene configurations, respectively.

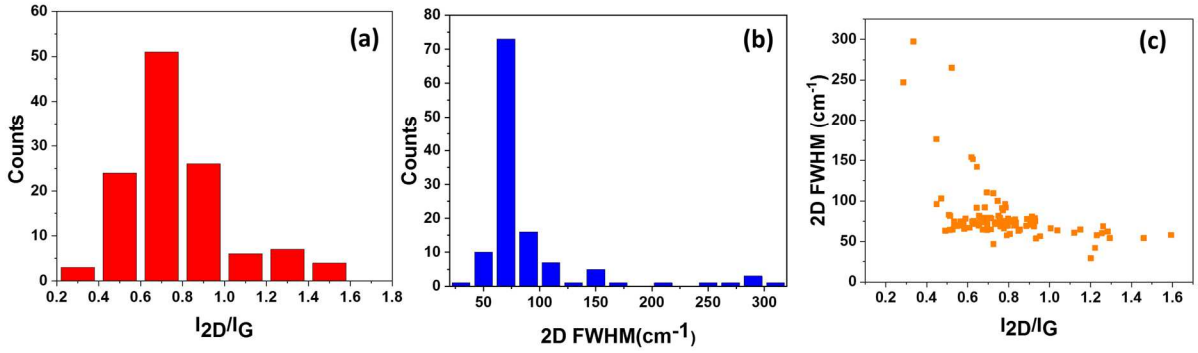

Figure 7: Histograms of (a) the I_{2D}/I_G intensity ratio and (b) I_D/I_G intensity ratio, both related to the 100 Raman spectra obtained for the mapping of the BG film; (c) FWHM(2D) peak plotted versus the I_{2D}/I_G ratio for the BG film, consistent with a boron-doped graphene film mainly constituted of 2-3 layers (see text for details).

The B/(B+C) %, deduced from XPS in both the a-C:B film precursor and in the BG graphene, is equal to 2.0 at.%, meaning that the annealing process transforming the a-C:B film into BG does not affect the concentration of boron during the conversion of the a-C:B film into the BG film. Thus controlling the boron concentration in the a-C:B film precursor during the PLD process ensures makes it possible to control the concentration of boron in the BG film, which is a considerable advantage in graphene synthesis procedures. Oxygen is present in the samples before and after annealing and can be attributed both to adventitious contamination and oxygen incorporation in the films due to residual water vapor in the PLD chamber (maintained near 10^{-4} Pa during deposition). The O1 signal is more intense in the BG film than in the a-C:B film, which is consistent with a higher reactivity of the BG film with oxygen during the RTA process at 1100 °C.

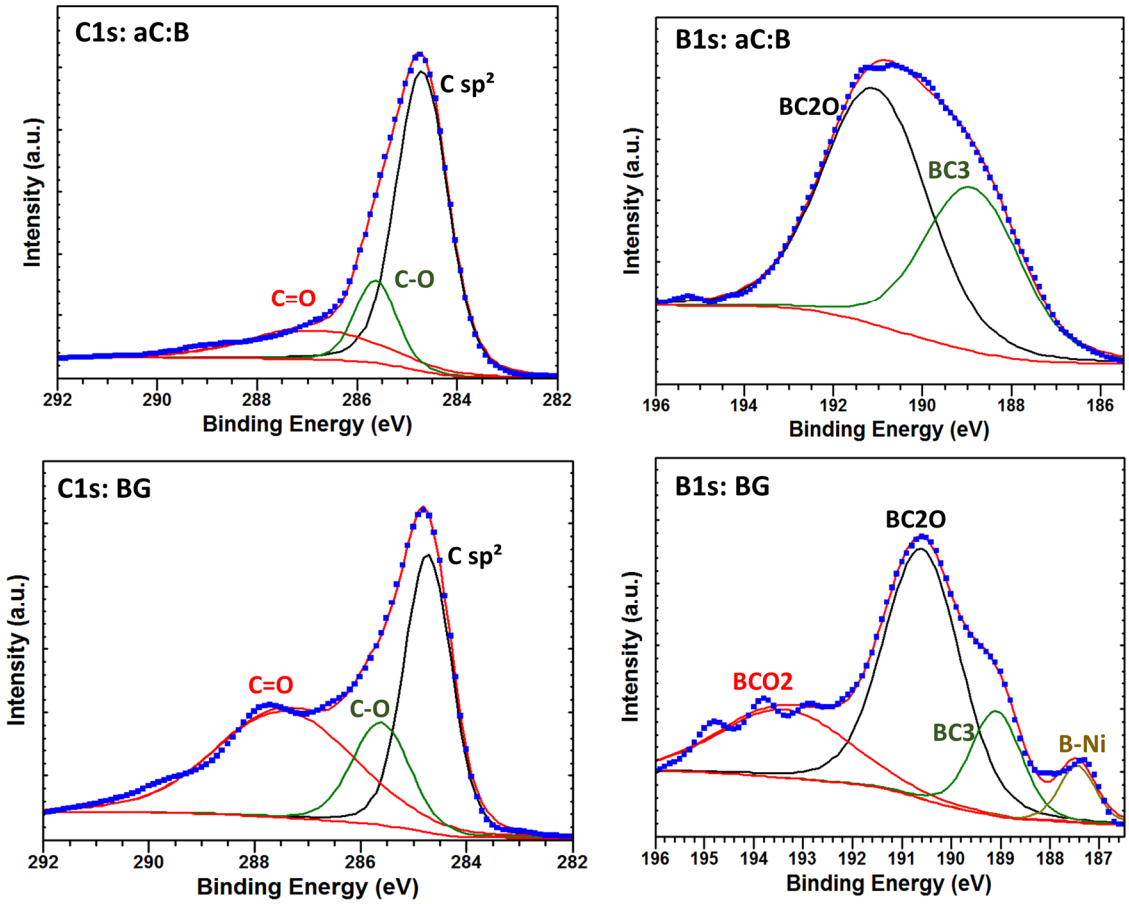

Figure 8: XPS C1s and B1s core levels of the a-C:B film precursor and boron-doped graphene film (BG) obtained by RTA of the a-C:B film at 1100 °C. The B/(B+C) ratio of the a-C:B film precursor and boron-doped graphene obtained by RTA is similar (2 at.%), showing that the synthesis process allows to control accurately the boron concentration in the graphene.

XPS spectra depicted in **Figure 8** compare the C1 and B1 core levels of the a-C:B film, as deposited by the co-ablation process of carbon and boron (i.e. before annealing allows its conversion into boron-doped graphene), with the C1 and B1 core levels of the boron-doped film obtained by RTA of the a-C:B film at 1100 °C. The peak deconvolutions and their exact interpretation are rather controversial (as discussed later), due to the proximity of electronic configuration of carbon and boron with a slight difference in their electronegativity, and due to the many chemical functions combining B, C and O species. Our interpretation of XPS is based on a compilation of previous published data related to boron-doped graphene and nickel-boride compounds**[12,22,23,28,40–42]**. In the a-C:B film, the C1 contributions, centered at 284.7, 285.8 and 285.3 eV, are respectively assigned to sp^2 carbon (typically observed in diamond-like carbon films), C-O and C=O species. The B1 contributions, centered at 188.9 and 191.1 eV, are assigned to BC_3 and BC_2O respectively. After conversion of the a-C:B film into the BG film by RTA, the position of the C1 contributions is not significantly

modified. Only a relative increase in the C-O and C=O contributions is observed, in agreement with the higher O1 contribution. Conversely, four B1 contributions can be introduced to fit the boron signal, centered at 187.4, 189.1, 190.6 and 193.4, assigned to B-Ni, BC_3, BC_2O, and BCO_2 respectively. These chemical functions were also observed by XPS in most of the references related to BG films cited above. Cattalan et al.**[22]** observed that BC_2O and BCO_2 are easily formed when B localizes in a low coordinated substitutional site along graphene edges. The relative abundance of oxygen in boron- and carbon-containing chemical groups is typical of top-surface compositions investigated by XPS.

The surface film morphologies, deduced from SEM, are depicted in **Figure 9**. On the Ni/SiO_2 film (**Figure 9a**), the RTA process induces the formation of spherical nodules of nickel, 50-300 nm in diameter, dispersed on the surface of the silica substrate. The a-C:B film (**Figure 9b**) appears strikingly smooth, as we already observed **[34]**. Compared to the pure annealed Ni film (**Figure 9a**), the size of the Ni nodules observed on the pure graphene layer (**Figure 9c**) increases to the micrometer range. This suggests that the presence of a thin carbonaceous film modifies the phenomenon at the origin of the particle synthesis. These island-shaped metallic Ni nodules were also previously observed by Banno et al.**[43]** and by Xiong et al.**[44]** with graphene grown in the presence of Ni catalyst, using RTA in the temperature range 900-1100 °C. This is consistent with the sublimation of the Ni layer during heating at a high temperature in vacuum.

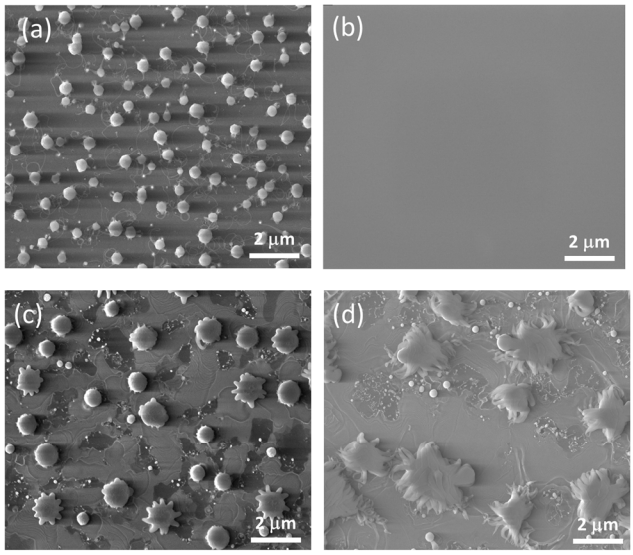

Figure 9: Surface morphology deduced from SEM related to (a) the Ni film with no carbon deposition after RTA at 1100°C for 2 minutes, (b) the initial a-C:B film prior to RTA, (c) the pure graphene film obtained from the a-C film annealed by RTA at 1100°C for 2 minutes and (d) the boron-doped graphene film (BG) obtained from the a-C:B film annealed by RTA at 1100°C for 2 minutes. All SEM figures were obtained with the same magnification (x 20 000).

Conversely, the BG film revealed larger Ni clusters whose lateral size ranged from 1 to 3 µm (**Figure 9d**) with a dramatic morphological change. Since the pure graphene surface and the BG surface underwent the same RTA process, the difference in the morphologies of the Ni clusters can be attributed to diffusion of boron atoms in the nickel, as revealed by XPS described above, showing the presence of B-Ni bonds. The resulting alloy might have different thermal properties leading to the different observed particle shapes. **Figure 10** shows the morphology of the large Ni clusters, with a RSM value of 338 nm, as observed by AFM on the BG film. The shape of the Ni clusters is consistent with the FEG-SEM observation.

Taking into consideration these results and interpretations, we show that an amorphous a-C:B film obtained by co-ablation of carbon and boron can be thermally converted into a boron-doped graphene film whose concentration in boron is fully controlled by the PLD process. Boron atoms are incorporated into the carbon network, as deduced from XPS investigations. The graphene film nanoarchitecture is not disturbed by the boron doping, in terms of surface

distribution of graphene layer number, as deduced from the Raman investigations. However, the boron incorporation induces a significant increase of defects attributed to a decrease, by a factor 4-5, of the size of the graphene clusters. The temperature achieved during the RTA process allows the partial vacuum sublimation of the Ni film catalyst, certainly accelerated by a de-wetting of nickel in contact with the initial PLD carbon-based film during heating. Further investigations will be dedicated to the incorporation of higher concentrations of boron and their effect typically on electronic conductions and electrochemical properties.

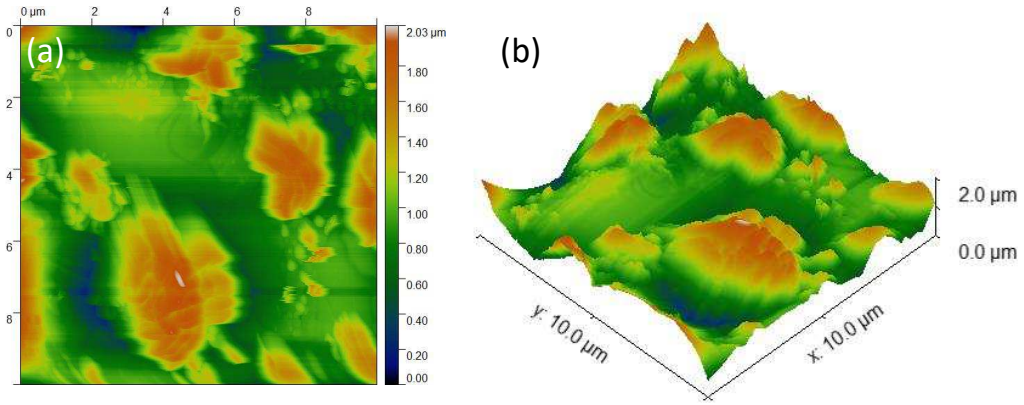

Figure 10: Surface morphology deduced from AFM of the boron-doped graphene film (BG) obtained from the a-C:B film annealed by RTA at 1100°C for 2 minutes (a) 2D image and (b) 3D image. The RMS value deduced from AFM is 338 nm. The nodules observed by SEM (Fig.9) are clearly visible by AFM which quantifies their influence on the surface morphology.

Conclusions

The present study demonstrates the synthesis of boron-doped graphene films by pulse laser co-ablation of carbon and boron in high vacuum conditions. The film nanoarchitecture and composition is investigated by combining Raman, XPS, SEM and HRTEM. The novelty of the results consists in the possibility to control accurately the boron concentration in the doped graphene films, by adjusting the boron concentration in the amorphous a-C:B film obtained by pulsed laser deposition, and converted into boron-doped graphene by rapid thermal annealing in low vacuum at 1100 °C, in the presence of a Ni catalyst layer. This represents a significant advantage over most other processes, including CVD processes. The boron-doped graphene film, within 1-4 layers, contains 2 at.% of boron predominantly bonded to carbon in both BC_3 and BC_2O configurations. The nanoarchitecture of the boron-doped graphene film is very similar than observed without any dopant, except an increase of the defect density

associated to a decrease of cluster size from 59 nm without boron to 22 nm with boron. The SiO_2 substrate covered by the BG film become highly transparent after the rapid thermal annealing process, due to the sublimation of most of the Ni film catalyst. This work offers perspectives to achieve a better control of electronic and chemical properties of sensors through robust boron doping of graphene films.

Acknowledgements

This work was supported by the LABEX MANUTECH-SISE (ANR-10-LABX-0075) of *Université de Lyon*, as part of the program "*Investissements d'Avenir*" (ANR-11-IDEX-0007) operated by the French National Research Agency (ANR).

References

[1] X. Wang, G. Sun, P. Routh, D.-H. Kim, W. Huang, P. Chen, Heteroatom-doped graphene materials: syntheses, properties, and applications, Chemical Society Reviews. 43 (2014) 7067–7098. doi:10.1039/C4CS00141A.

[2] S. Agnoli, M. Favaro, Doping graphene with boron: a review of synthesis methods, physicochemical characterization, and emerging applications, J. Mater. Chem. A. 4 (2016) 5002–5025. doi:10.1039/C5TA10599D.

[3] L. Tsetseris, S.T. Pantelides, Graphene: An impermeable or selectively permeable membrane for atomic species?, Carbon. 67 (2014) 58–63. doi:10.1016/j.carbon.2013.09.055.

[4] P. Rani, V.K. Jindal, Designing band gap of graphene by B and N dopant atoms, RSC Adv. 3 (2012) 802–812. doi:10.1039/C2RA22664B.

[5] X. Lü, J. Wu, T. Lin, D. Wan, F. Huang, X. Xie, M. Jiang, Low-temperature rapid synthesis of high-quality pristine or boron-doped graphenevia Wurtz-type reductive coupling reaction, J. Mater. Chem. 21 (2011) 10685–10689. doi:10.1039/C1JM11184A.

[6] J. Han, L.L. Zhang, S. Lee, J. Oh, K.-S. Lee, J.R. Potts, J. Ji, X. Zhao, R.S. Ruoff, S. Park, Generation of B-Doped Graphene Nanoplatelets Using a Solution Process and Their Supercapacitor Applications, ACS Nano. 7 (2013) 19–26. doi:10.1021/nn3034309.

[7] S. Umrao, T.K. Gupta, S. Kumar, V.K. Singh, M.K. Sultania, J.H. Jung, I.-K. Oh, A. Srivastava, Microwave-Assisted Synthesis of Boron and Nitrogen co-doped Reduced Graphene Oxide for the Protection of Electromagnetic Radiation in Ku-Band, ACS Appl. Mater. Interfaces. 7 (2015) 19831–19842. doi:10.1021/acsami.5b05890.

[8] V. Thirumal, A. Pandurangan, R. Jayavel, R. Ilangovan, Synthesis and characterization of boron doped graphene nanosheets for supercapacitor applications, Synthetic Metals. 220 (2016) 524–532. doi:10.1016/j.synthmet.2016.07.011.

[9] L.S. Panchakarla, K.S. Subrahmanyam, S.K. Saha, A. Govindaraj, H.R. Krishnamurthy, U.V. Waghmare, C.N.R. Rao, Synthesis, Structure, and Properties of Boron- and Nitrogen-Doped Graphene, Advanced Materials. 21 (2009) 4726–4730. doi:10.1002/adma.200901285.

[10] Z.-S. Wu, W. Ren, L. Xu, F. Li, H.-M. Cheng, Doped Graphene Sheets As Anode Materials with Superhigh Rate and Large Capacity for Lithium Ion Batteries, ACS Nano. 5 (2011) 5463–5471. doi:10.1021/nn2006249.
[11] Y.A. Kim, K. Fujisawa, H. Muramatsu, T. Hayashi, M. Endo, T. Fujimori, K. Kaneko, M. Terrones, J. Behrends, A. Eckmann, C. Casiraghi, K.S. Novoselov, R. Saito, M.S. Dresselhaus, Raman Spectroscopy of Boron-Doped Single-Layer Graphene, ACS Nano. 6 (2012) 6293–6300. doi:10.1021/nn301728j.
[12] Z.-H. Sheng, H.-L. Gao, W.-J. Bao, F.-B. Wang, X.-H. Xia, Synthesis of boron doped graphene for oxygen reduction reaction in fuel cells, J. Mater. Chem. 22 (2011) 390–395. doi:10.1039/C1JM14694G.
[13] L. Wang, Z. Sofer, P. Šimek, I. Tomandl, M. Pumera, Boron-Doped Graphene: Scalable and Tunable p-Type Carrier Concentration Doping, J. Phys. Chem. C. 117 (2013) 23251–23257. doi:10.1021/jp405169j.
[14] H. Fang, C. Yu, T. Ma, J. Qiu, Boron-doped graphene as a high-efficiency counter electrode for dye-sensitized solar cells, Chem. Commun. 50 (2014) 3328–3330. doi:10.1039/C3CC48258H.
[15] B.R. Sathe, X. Zou, T. Asefa, Metal-free B-doped graphene with efficient electrocatalytic activity for hydrogen evolution reaction, Catal. Sci. Technol. 4 (2014) 2023–2030. doi:10.1039/C4CY00075G.
[16] G. Jo, J. Sanetuntikul, S. Shanmugam, Boron and phosphorous-doped graphene as a metal-free electrocatalyst for the oxygen reduction reaction in alkaline medium, RSC Adv. 5 (2015) 53637–53643. doi:10.1039/C5RA06952A.
[17] Z. Peng, R. Ye, J.A. Mann, D. Zakhidov, Y. Li, P.R. Smalley, J. Lin, J.M. Tour, Flexible Boron-Doped Laser-Induced Graphene Microsupercapacitors, ACS Nano. 9 (2015) 5868–5875. doi:10.1021/acsnano.5b00436.
[18] D.-Y. Yeom, W. Jeon, N.D.K. Tu, S.Y. Yeo, S.-S. Lee, B.J. Sung, H. Chang, J.A. Lim, H. Kim, High-concentration boron doping of graphene nanoplatelets by simple thermal annealing and their supercapacitive properties, Scientific Reports. 5 (2015) 9817. doi:10.1038/srep09817.
[19] M. Telychko, P. Mutombo, P. Merino, P. Hapala, M. Ondráček, F.C. Bocquet, J. Sforzini, O. Stetsovych, M. Vondráček, P. Jelínek, M. Švec, Electronic and Chemical Properties of Donor, Acceptor Centers in Graphene, ACS Nano. 9 (2015) 9180–9187. doi:10.1021/acsnano.5b03690.
[20] W. Norimatsu, K. Hirata, Y. Yamamoto, S. Arai, M. Kusunoki, Epitaxial growth of boron-doped graphene by thermal decomposition of B4C, J. Phys.: Condens. Matter. 24 (2012) 314207. doi:10.1088/0953-8984/24/31/314207.
[21] X. Li, L. Fan, Z. Li, K. Wang, M. Zhong, J. Wei, D. Wu, H. Zhu, Boron Doping of Graphene for Graphene–Silicon p–n Junction Solar Cells, Advanced Energy Materials. 2 (2012) 425–429. doi:10.1002/aenm.201100671.
[22] M. Cattelan, S. Agnoli, M. Favaro, D. Garoli, F. Romanato, M. Meneghetti, A. Barinov, P. Dudin, G. Granozzi, Microscopic View on a Chemical Vapor Deposition Route to Boron-Doped Graphene Nanostructures, Chem. Mater. 25 (2013) 1490–1495. doi:10.1021/cm302819b.
[23] H. Wang, Y. Zhou, D. Wu, L. Liao, S. Zhao, H. Peng, Z. Liu, Synthesis of Boron-Doped Graphene Monolayers Using the Sole Solid Feedstock by Chemical Vapor Deposition, Small. 9 (2013) 1316–1320. doi:10.1002/smll.201203021.

[24] L. Zhao, M. Levendorf, S. Goncher, T. Schiros, L. Pálová, A. Zabet-Khosousi, K.T. Rim, C. Gutiérrez, D. Nordlund, C. Jaye, M. Hybertsen, D. Reichman, G.W. Flynn, J. Park, A.N. Pasupathy, Local Atomic and Electronic Structure of Boron Chemical Doping in Monolayer Graphene, Nano Lett. 13 (2013) 4659–4665. doi:10.1021/nl401781d.
[25] D.Yu. Usachov, A.V. Fedorov, A.E. Petukhov, O.Yu. Vilkov, A.G. Rybkin, M.M. Otrokov, A. Arnau, E.V. Chulkov, L.V. Yashina, M. Farjam, V.K. Adamchuk, B.V. Senkovskiy, C. Laubschat, D.V. Vyalikh, Epitaxial B-Graphene: Large-Scale Growth and Atomic Structure, ACS Nano. 9 (2015) 7314–7322. doi:10.1021/acsnano.5b02322.
[26] M. Ovezmyradov, I.V. Magedov, L.V. Frolova, G. Chandler, J. Garcia, D. Bethke, E.A. Shaner, N.G. Kalugin, Chemical Vapor Deposition of Phosphorous- and Boron-Doped Graphene Using Phenyl-Containing Molecules, J Nanosci Nanotechnol. 15 (2015) 4883–4886. doi:10.1166/jnn.2015.9827.
[27] L. Wang, X. Zhang, F. Yan, H.L.W. Chan, F. Ding, Mechanism of boron and nitrogen in situ doping during graphene chemical vapor deposition growth, Carbon. 98 (2016) 633–637. doi:10.1016/j.carbon.2015.11.058.
[28] Y. You, C. Wang, Y.L. Xu, J.X. Wan, W. Ren, X.H. Fang, X.Y. Chen, Effects of growth conditions on the quality of B-doped graphene films, Journal of Applied Physics. 121 (2017) 025305. doi:10.1063/1.4974010.
[29] D.W. Boukhvalov, I.S. Zhidkov, A.I. Kukharenko, A.I. Slesarev, A.F. Zatsepin, S.O. Cholakh, E.Z. Kurmaev, Stability of boron-doped graphene/copper interface: DFT, XPS and OSEE studies, Applied Surface Science. 441 (2018) 978–983. doi:10.1016/j.apsusc.2018.02.074.
[30] G.V. Soares, S. Nakhaie, M. Heilmann, H. Riechert, J.M.J. Lopes, Growth of boron-doped few-layer graphene by molecular beam epitaxy, Appl. Phys. Lett. 112 (2018) 163103. doi:10.1063/1.5019352.
[31] Y. Bleu, F. Bourquard, T. Tite, A.-S. Loir, C. Maddi, C. Donnet, F. Garrelie, Review of Graphene Growth From a Solid Carbon Source by Pulsed Laser Deposition (PLD), Front Chem. 6 (2018). doi:10.3389/fchem.2018.00572.
[32] C. Maddi, F. Bourquard, V. Barnier, J. Avila, M.-C. Asensio, T. Tite, C. Donnet, F. Garrelie, Nano-Architecture of nitrogen-doped graphene films synthesized from a solid CN source, Scientific Reports. 8 (2018) 3247. doi:10.1038/s41598-018-21639-9.
[33] F. Bourquard, Y. Bleu, A.-S. Loir, B. Caja-Munoz, J. Avila, M.-C. Asensio, G. Raimondi, M. Shokouhi, I. Rassas, C. Farre, C. Chaix, V. Barnier, N. Jaffrezic-Renault, F. Garrelie, C. Donnet, Electroanalytical Performance of Nitrogen-Doped Graphene Films Processed in One Step by Pulsed Laser Deposition Directly Coupled with Thermal Annealing, Materials. 12 (2019) 666. doi:10.3390/ma12040666.
[34] A. Sikora, O. Bourgeois, J.C. Sanchez-Lopez, J.-N. Rouzaud, T.C. Rojas, A.-S. Loir, J.-L. Garden, F. Garrelie, C. Donnet, Effect of boron incorporation on the structure and electrical properties of diamond-like carbon films deposited by femtosecond and nanosecond pulsed laser ablation, Thin Solid Films. 518 (2009) 1470–1474. doi:10.1016/j.tsf.2009.09.111.
[35] A.C. Ferrari, J.C. Meyer, V. Scardaci, C. Casiraghi, M. Lazzeri, F. Mauri, S. Piscanec, D. Jiang, K.S. Novoselov, S. Roth, A.K. Geim, Raman Spectrum of Graphene and Graphene Layers, Phys. Rev. Lett. 97 (2006) 187401. doi:10.1103/PhysRevLett.97.187401.
[36] A.C. Ferrari, Raman spectroscopy of graphene and graphite: Disorder, electron–phonon coupling, doping, and nonadiabatic effects, Solid State Communications. 143 (2007) 47–57. doi:10.1016/j.ssc.2007.03.052.

[37] L.M. Malard, M.A. Pimenta, G. Dresselhaus, M.S. Dresselhaus, Raman spectroscopy in graphene, Physics Reports. 473 (2009) 51–87. doi:10.1016/j.physrep.2009.02.003.
[38] F. Tuinstra, J.L. Koenig, Raman Spectrum of Graphite, J. Chem. Phys. 53 (1970) 1126–1130. doi:10.1063/1.1674108.
[39] C.H. Lui, Z. Li, Z. Chen, P.V. Klimov, L.E. Brus, T.F. Heinz, Imaging Stacking Order in Few-Layer Graphene, Nano Lett. 11 (2011) 164–169. doi:10.1021/nl1032827.
[40] J. Legrand, S. Gota, M.-J. Guittet, C. Petit, Synthesis and XPS Characterization of Nickel Boride Nanoparticles, Langmuir. 18 (2002) 4131–4137. doi:10.1021/la0117247.
[41] M. Sahoo, K.P. Sreena, B.P. Vinayan, S. Ramaprabhu, Green synthesis of boron doped graphene and its application as high performance anode material in Li ion battery, Materials Research Bulletin. 61 (2015) 383–390. doi:10.1016/j.materresbull.2014.10.049.
[42] Y. Sun, C. Du, M. An, L. Du, Q. Tan, C. Liu, Y. Gao, G. Yin, Boron-doped graphene as promising support for platinum catalyst with superior activity towards the methanol electrooxidation reaction, Journal of Power Sources. 300 (2015) 245–253. doi:10.1016/j.jpowsour.2015.09.046.
[43] K. Banno, M. Mizuno, K. Fujita, T. Kubo, M. Miyoshi, T. Egawa, T. Soga, Transfer-free graphene synthesis on insulating substrates via agglomeration phenomena of catalytic nickel films, Appl. Phys. Lett. 103 (2013) 082112. doi:10.1063/1.4818342.
[44] W. Xiong, Y.S. Zhou, W.J. Hou, T. Guillemet, J.F. Silvain, Y. Gao, M. Lahaye, E. Lebraud, S. Xu, X.W. Wang, D.A. Cullen, K.L. More, L. Jiang, Y.F. Lu, Solid-state graphene formation via a nickel carbide intermediate phase, RSC Adv. 5 (2015) 99037–99043. doi:10.1039/C5RA18682J.

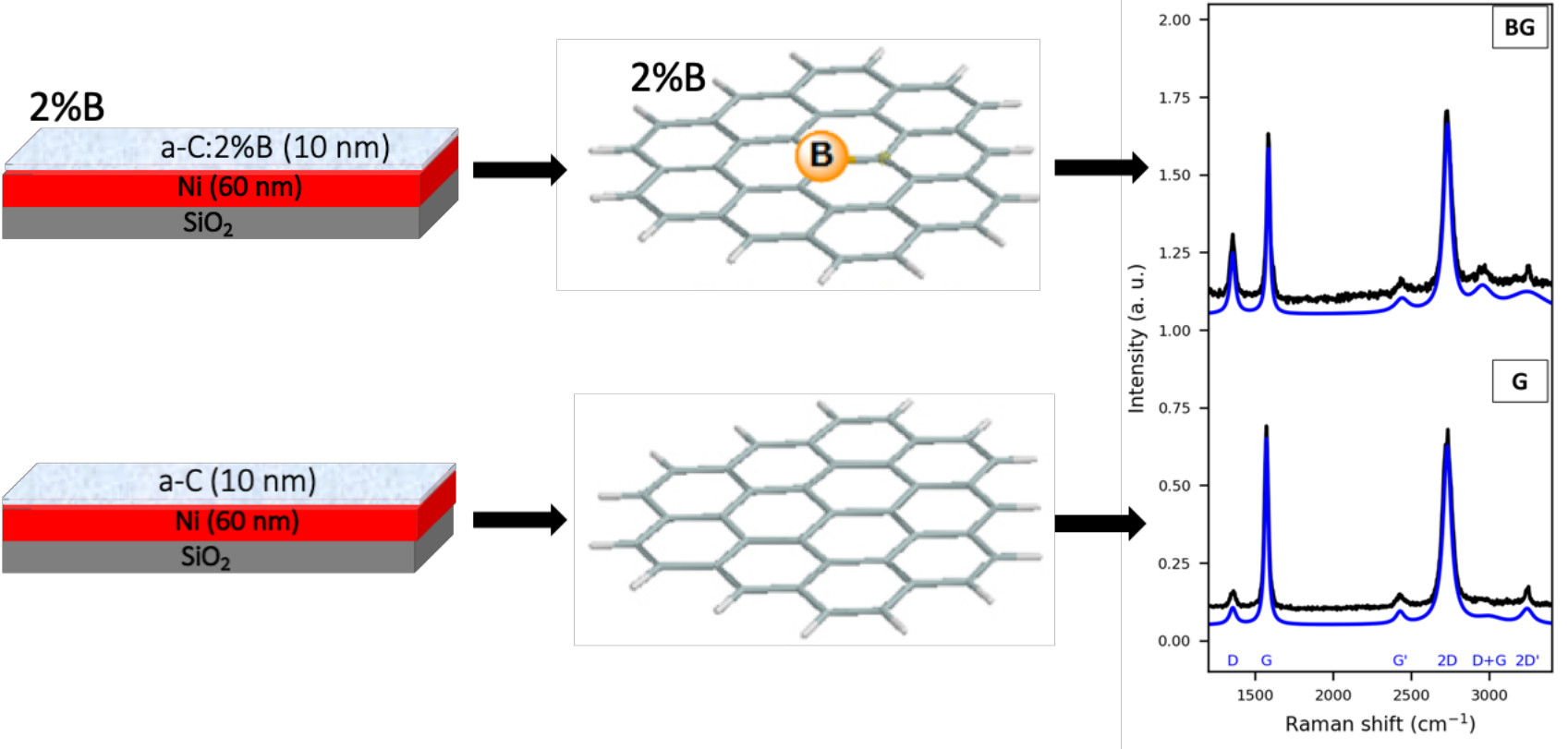
2%B
a-C:2%B (10 nm)
Ni (60 nm)
SiO2
2%B
B
a-C (10 nm)
Ni (60 nm)
SiO2
BG
G
Intensity (a. u.)
Raman shift (cm−1)
D
G
G'
2D
D+G
2D'